

**Atomic-scale structure of Co-Pt bimetallic nanoparticles: Monte Carlo simulations**Lijia Qin,<sup>1</sup> Yonghong Zhang,<sup>2</sup> Shiping Huang,<sup>1,\*</sup> Huiping Tian,<sup>3</sup> and Peng Wang<sup>3</sup><sup>1</sup>*Division of Molecule and Materials Simulation, Key Laboratory for Nanomaterials, Ministry of Education, Beijing University of Chemical Technology, Beijing 100029, China*<sup>2</sup>*Department of Physics, Tianjin Polytechnic University, Tianjin 300160, China*<sup>3</sup>*Research Institute of Petroleum Processing, SINOPEC, Beijing 100083, China*

(Received 14 March 2010; revised manuscript received 19 July 2010; published 11 August 2010)

Co-Pt bimetallic nanoparticles (NPs) with icosahedral, decahedral, and truncated octahedral morphologies are obtained by using effective semigrand canonical ensemble Monte Carlo simulation, which is based on the second-moment approximation of the tight-binding potential. The simulation results show that Co atoms occupy first the central site, then diagonal lines or adjacent vertices positions, finally the vertices and edges as the Co mole fraction increases. We also study the binding-energy difference to investigate the relative structural stability of Co-Pt bimetallic nanoparticles. Atomic-scale structural properties are investigated by structure function and atomic pair-distribution function technologies. In the nanoparticles with about 0.50 Co mole fraction at 100 K, the first-neighbor Co-Co, Co-Pt, and Pt-Pt distances are 2.51–2.54( $\pm 0.01$ ) Å, 2.57–2.58( $\pm 0.01$ ) Å, and 2.64–2.68( $\pm 0.01$ ) Å, respectively, which are all consistent with experimental values of around 2 nm NPs. The simulation results also show that the morphology, composition, and temperature play an important role in the atomic-scale structural properties of the Co-Pt bimetallic nanoparticles.

DOI: [10.1103/PhysRevB.82.075413](https://doi.org/10.1103/PhysRevB.82.075413)

PACS number(s): 61.46.Bc, 68.35.bd, 82.20.Wt

**I. INTRODUCTION**

In recent years, a lot of experimental and theoretical efforts have been put into nanomaterials due to their dramatically physical and chemical properties different from bulk materials.<sup>1</sup> Especially, bimetallic nanoparticles (NPs) are one kind of these novel nanomaterials. Since the useful physical and chemical properties, bimetallic NPs have been applied extensively in many fields, such as electronics, magnetism, optics, and chemical catalysis.<sup>1–5</sup> The physicochemical properties depend distinctly on their structure, chemical composition, and temperature. Structure and chemical composition have already attracted much attention both from experimental<sup>6</sup> and theoretical<sup>7–12</sup> studies recently. There are three common structures observed in these studies, that is, icosahedron, decahedron, and truncated octahedron.<sup>13</sup> Other unconventional structures such as dodecahedron and planar are also generated by recent literatures.<sup>14–19</sup> It is also reported that Co-Pt bimetallic NPs with Pt: Co atomic ratio of 1:1 or 3:1 present very high catalytic activity.<sup>20</sup>

Considerable experimental efforts have been put into synthesis and characterization of Co-Pt bimetallic NPs.<sup>7,21–26</sup> Co-Pt alloy films are synthesized by Lin and Gorman<sup>7</sup> using e-beam evaporation at substrate temperatures near 200 °C. It is found that the perpendicular magnetic anisotropy is related strongly to the good Co-Pt (111) texture. CoPt<sub>3</sub> NPs are also made by using NaBH<sub>4</sub> as a reductant,<sup>27</sup> and their results show the CoPt<sub>3</sub> NPs have a face-centered-cubic (fcc) crystalline structure with an average particle size of 2.6 nm. Many experimental tools are used to characterize the structures or properties of Co-Pt bimetallic NPs, such as thermogravimetry, differential thermal analysis, Fourier transform infrared, transmission electron microscopy, and x-ray diffraction (XRD). Phase transition of the Co<sub>core</sub>Pt<sub>shell</sub> NPs from fcc to face-centered tetragonal at annealing temperature above 550 °C is confirmed by electron and x-ray diffraction

patterns.<sup>1</sup> In addition, structure transition from icosahedron to fcc during growth is observed by grazing incidence (GI) small-angle x-ray scattering and grazing GIXRD.<sup>13</sup> However, XRD pattern often shows a few peaks when it is applied in NPs system. These poor-quality peaks make the traditional technique unsuitable in structural characterization of atomic-scale NPs. It is reported that high-energy XRD coupled to atomic pair-distribution function (PDF) analysis is suited for the structural study of materials at nanoscale.<sup>6,28–40</sup> In addition, the PDF method can be used not only in experiment but also in computer molecule simulation technology.<sup>41</sup>

The structural properties of Co-Pt bimetallic NPs are also studied by many theoretical methods. Kinetic Monte Carlo (MC) method is used to simulate the Co-Pt film growth process.<sup>42</sup> Global optimization and Monte Carlo simulation based on tight-binding potential are both adopted by Rossi *et al.*<sup>43</sup> They observed that polyicosahedronlike, decahedron, and fcc structures are the most stable for Co-Pt bimetallic clusters with atom number  $N < 100$ ,  $100 < N < 400$ , and  $400 < N < 1000$ , respectively. Molecular-dynamics method is carried out to simulate the growth process of isolated Co clusters in gas phase. Good agreements both for the geometric structures and for the behavior of lattice contraction are obtained by simulation results though comparing with experiment, density-functional theory, and semiempirical calculations.<sup>44</sup> Density-functional theory is also used to study the geometrical and magnetic properties of (CoPt)<sub>*n*</sub> ( $1 \leq n \leq 5$ ) bimetallic clusters.<sup>45</sup>

However, only a few research works have revealed the effects of different morphologies, compositions, and temperatures on the atomic-scale structural properties of Co-Pt bimetallic NPs. For this purpose, we initially perform Monte Carlo simulation based on a many-body potential derived from the tight-binding model. Three different morphologies: icosahedron (Ico type with 561 atoms), decahedron (Dec type with 561 atoms), and truncated octahedron (TOh type with 711 atoms) are all adopted. Then, all coordinates of

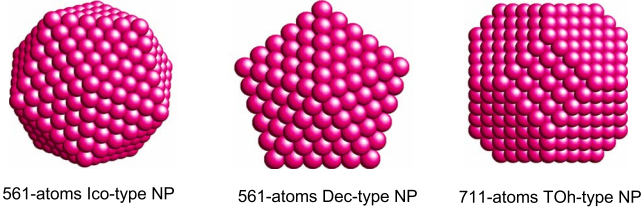


FIG. 1. (Color online) Snapshots of three initial morphologies.

simulation results are collected and transformed by the atomic PDF technique into the atomic-scale structural properties. In this work, the computational models including initial NPs configurations, tight-binding potential, and Monte Carlo simulation details are described briefly in Sec. II. Numerical methods for the Debye equation and atomic pair-distribution function calculated from atomic configurations are presented in Sec. III. The results for morphology, composition, and temperature effects on atomic-level structural properties are discussed in Sec. IV.

## II. COMPUTATIONAL DETAILS

### A. Initial NPs configurations

The initial atomic configurations of Co-Pt bimetallic NPs with icosahedral, decahedral, and truncated octahedral morphologies are taken from the work of Turner *et al.*<sup>46</sup> These initial morphologies contain 561, 561, and 711 atoms, respectively. Snapshots of these initial morphologies are shown in Fig. 1. Before starting the Monte Carlo runs, a relatively short steepest-descent minimization is performed to relax the lattice in the initial configurations. It is noticed that, in fact, the initial configurations can be generated in different ways without influencing the final configurations of the NPs of interest.

### B. Empirical Gupta many-body potential

Atom-atom interactions are modeled by the empirical Gupta many-body potential, which is based on the second-moment approximation of the tight-binding (TB-SMA) potential.<sup>47</sup> This potential has been shown to be highly accurate in modeling of both metal alloys<sup>48</sup> and monometallic and bimetallic NPs.<sup>10,49,50</sup> Moreover, this potential has the ability of accounting for the surface relaxations and reconstructions, so it is ideal for the model of Co-Pt bimetallic NPs.<sup>42,51,52</sup> Within the TB-SMA potential, the total energy of a system with  $N$  atoms is expressed as follows:

$$E_{total} = \sum_{i=1}^N (E_R^i + E_B^i), \quad (1)$$

where the total energy  $E_{total}$  is a sum of two terms: a repulsive term  $E_R^i$  of Born-Mayer type and an attractive term  $E_B^i$  of band originated from the band structure.  $E_R^i$  and  $E_B^i$  can be written, respectively, as

$$E_R^i = \sum_{i \neq j} A_{ij} \exp \left[ -p_{ij} \left( \frac{r_{ij}}{r_0} \right) - 1 \right], \quad (2)$$

TABLE I. Parameters of TB-SMA potential for the Co-Pt bimetallic NPs.

	$A_{ij}$ (eV)	$\xi_{ij}$ (eV)	$p_{ij}$	$q_{ij}$	$r_0$ (Å)
Co-Co	0.189	1.907	8.80	2.96	2.50
Co-Pt	0.245	2.386	9.97	3.32	2.63
Pt-Pt	0.242	2.506	11.14	3.68	2.76

$$E_B^i = - \left\{ \sum_{i \neq j} \xi_{ij}^2 \exp \left[ -2q_{ij} \left( \frac{r_{ij}}{r_0} - 1 \right) \right] \right\}^{1/2}, \quad (3)$$

where  $i$  and  $j$  represent the chemical nature of atom  $i$  and  $j$ , respectively.  $r_{ij}$  is the interatomic distance between atom  $i$  and  $j$  in NPs while  $r_0$  is the first-neighbor distance  $r_i$  in pure metals ( $i=j$ ) or the average first-neighbor distance  $r_0 = \frac{r_{ii} + r_{jj}}{2}$  between two pure metals ( $i \neq j$ ). In this study, parameters  $A_{ij}$ ,  $\xi_{ij}$ ,  $p_{ij}$ ,  $q_{ij}$ , and  $r_0$  of the TB-SMA potential are taken from the literature<sup>52</sup> and listed in Table I. These parameters have been employed for the theoretical study of Co-Pt bimetallic NPs with satisfying results.<sup>52</sup> In order to investigate the structural stability, we define the average binding energy  $E_b$  as the negative quantity of averaged  $E_{total}$  for  $N$ -atom system

$$E_b = \frac{-E_{total}}{N}. \quad (4)$$

### C. Monte Carlo simulations

MC simulations of Co-Pt bimetallic NPs are performed in the semigrand-canonical ensemble,<sup>53,54</sup> in which the total number of atoms ( $N = N_{Co} + N_{Pt}$ ), temperature ( $T$ ), and chemical potential difference ( $\Delta\mu = \mu_{Pt} - \mu_{Co}$ ) between the two species are fixed. The algorithm allows the number of atoms of each species to vary. The chemical composition at a given temperature is therefore obtained by performing the MC simulation at a fixed value of chemical-potential difference  $\Delta\mu$  between the two species. For the bimetallic NPs, the MC simulation method includes two types of trial. (1) A small displacement of a randomly selected atom from its original position in a random direction, which corresponds to the relaxation and vibration processes. The magnitude of the displacement is in the range  $(0, r_{max})$ . The maximum displacement  $r_{max}$  is dynamically adjusted in order to maintain the acceptance rate of new configurations close to 0.5. (2) Random selection of the chemical type of an atom, corresponding to the fixed chemical-potential difference  $\Delta\mu$  between the two species and allowing the system to reach compositional equilibrium. With this method, the segregation can be well predicted at surfaces<sup>55-58</sup> and interfaces.<sup>59</sup> Moreover, the similar algorithm is proved to be successful in the study of the surface segregation of bimetallic nanoparticles.<sup>60,61</sup> This method is also used to obtain Co-Pt bimetallic NPs.

In our MC simulations,  $10^8$  steps are adopted for the total simulation length to achieve the most stable structure. The former  $5 \times 10^7$  steps are performed to make the system

equilibrium while the latter  $5 \times 10^7$  steps are used to obtain statistical structural properties such as atomic PDF.

### III. PDF TECHNIQUE

As a frequently used method to investigate the atomic-level structural properties, the PDF technique has been applied to the order and disorder analysis of bulk materials and NPs.<sup>6,28–40</sup> In order to obtain the PDF, atomic coordinates are all used for quantitative calculating the scattering intensity based on the Debye equation, which is used widely to the structural analysis.<sup>62–64</sup> The Debye equation is described as follows:

$$I(Q) = D^* \sum_{i=1} \sum_{j>i} f_i(Q) f_j(Q) \frac{\sin Qr_{ij}}{Qr_{ij}}, \quad (5)$$

where  $D^*$  is the Debye-Waller factor,  $r_{ij}$  is the interatomic distance between the atoms  $i$  and  $j$ , and  $Q$  is the magnitude of scattering vector

$$Q = 4\pi(\sin \theta)/\lambda, \quad (6)$$

where  $\theta$  is half of the angle between the incoming and outgoing x rays and  $\lambda$  is the wavelength of the x ray used, respectively.<sup>34</sup>  $f(Q)$  in Eq. (5) represents the atomic scattering form factor and can be written approximatively in an expression as follows:

$$f(Q) = 4\pi f[(\sin \theta)/\lambda] = 4\pi \left\{ \sum_{i=1}^4 a_i \exp[-b_i(\sin^2 \theta)/\lambda^2] + c \right\}, \quad (7)$$

where  $a_i$ ,  $b_i$ , and  $c$  are fitting constant coefficients taken from the International Tables for Crystallography.<sup>65</sup> These fitting coefficients have been found in effectively estimating the values of the atomic scattering form factor.<sup>66</sup> It should be mentioned that the value of  $f(Q)$  equals to the electrons number itself at zero scattering angle.

Another important item to obtain PDF is the structure function  $S(Q)$ ,<sup>39</sup> which can be generalized from the Debye equation  $I(Q)$  by dividing the expression  $\sum_{i=1}^N [c_i^2 f_i^2(Q)]$ ,

$$S(Q) = \frac{I(Q)}{\sum_{i=1}^N [c_i^2 f_i^2(Q)]} = 1 + D^* \frac{2}{\sum_{i=1}^N [c_i^2 f_i^2(Q)]} \times \sum_{i=1} \sum_{j>i} c_i c_j f_i(Q) f_j(Q) \frac{\sin Qr_{ij}}{Qr_{ij}}, \quad (8)$$

where  $c_i$  is the atomic concentration of species  $i$  ( $c_i = N_i/N_{total}$ ). Then, the structure function  $S(Q)$  can turn into the corresponding PDF  $G(r)$  via Fourier transformation, which can be expressed as follows:

$$G(r) = \left( \frac{2}{\pi} \right) \int_0^{Q=\max} Q [S(Q) - 1] \sin(Qr) dQ. \quad (9)$$

As can be seen from Eqs. (5)–(9), the PDF reflects both the long-range atomic order and local structural imperfection in

nanomaterials. Also, the PDF does not require periodic boundary condition in simulation methods. These advantages make the new technique excellent application in NPs system for atomic-scale structural properties analysis.

## IV. RESULTS AND DISCUSSION

### A. Structural properties

The snapshots of Co-Pt bimetallic NPs obtained by MC simulations are shown in Table II. It is found that Co atoms prefer to occupy the inside and Pt atoms are generally lying on the surface. This phenomenon, which is also observed by previous experimental<sup>1,67</sup> and theoretical<sup>68,69</sup> studies showing that the Co-Pt bimetallic NPs have a perfect core-shell structure with Co atoms in the core site, attributes mainly to the surface-energy difference between Co and Pt species. In other words, the enrichment of Pt atoms on surface leads to surface-energy minimization to keep stable geometrical structure. By analysis of Ico-type snapshots, it is found that Co atoms would like to occupy the central site and diagonal lines at 9% Co mole fraction in  $\text{Co}_{48}\text{Pt}_{513}$ . In  $\text{Co}_{90}\text{Pt}_{471}$ , Co atoms have already taken the main diagonal lines without appearing on the surface, showing a symmetrical structure along one centerline. When Co mole fraction reaches 43% in  $\text{Co}_{243}\text{Pt}_{318}$ , Co atoms begin to occupy the vertices and edges. More and more vertices and edges are occupied by Co atoms in  $\text{Co}_{344}\text{Pt}_{217}$ . Finally, there are only a few independent Pt atoms observed on the surface of  $\text{Co}_{490}\text{Pt}_{71}$  with symbol ‘‘B’’ in Table II. In the case of Dec-type snapshots, Co atoms occupy the central site and adjacent vertices positions in  $\text{Co}_{21}\text{Pt}_{540}$ . When Co mole fraction reaches 19% in  $\text{Co}_{107}\text{Pt}_{454}$ , most of the adjacent vertices and midpoints of edges are taken by Co atoms. As the increase in Co mole fraction, Co atoms appear at the vertices in  $\text{Co}_{146}\text{Pt}_{415}$ . It is noticed that a regular morphology cannot be kept by  $\text{Co}_{485}\text{Pt}_{76}$  with  $\Delta\mu=0.8$  eV, which maybe results from an energy-driven and entropy-driven effect. It is also observed in TOh-type snapshots that Co atoms occupy completely a diagonal line without appearing at the vertices in  $\text{Co}_{57}\text{Pt}_{654}$ . Another interesting phenomenon is that Co and Pt atoms arrange alternately in partial  $\text{Co}_{337}\text{Pt}_{374}$  with 47% Co mole fraction, showing a pseudo- $\text{L1}_0$ -ordered phase. The pseudo- $\text{L1}_0$ -ordered phase is also obtained on the (100) facets of  $\text{Co}_{493}\text{Pt}_{218}$  with 31% Co mole fraction (see Fig. 11, Ref. 72). The observation of pseudo- $\text{L1}_0$ -ordered phase is well consistent with previous studies.<sup>43,68</sup> In a word, as the increase in Co mole fraction in Ico-type, Dec-type, and TOh-type snapshots, Co atoms occupy first the central site, then diagonal lines or adjacent vertices positions, finally the vertices and edges.

Average binding energy  $E_b$  has been used to investigate the stability of NPs.<sup>70</sup> In this work,  $E_b$  is also studied on Co-Pt bimetallic NPs with a Co:Pt atomic ratio of 1:3 and listed in Table III. It is found that our computational  $E_b$  is in the range of 5.33–5.37 eV, which is consistent with experimental value.<sup>71</sup> On the basis of the accurate  $E_b$ , the binding-energy difference  $\Delta E_{b(\text{Dec-Ico})}$  is also performed and described as follows:

TABLE II. (Color online) Snapshots of Ico-type, Dec-type, and TOh-type Co-Pt bimetallic NPs with  $\Delta\mu=0.2-1.0$  eV at 100 K. Co and Pt atoms are represented as gray and pink spheres, respectively.




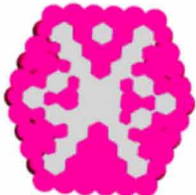





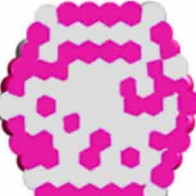
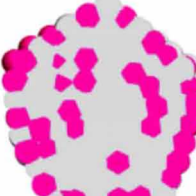
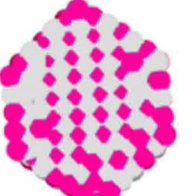
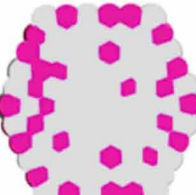
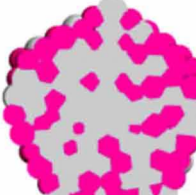
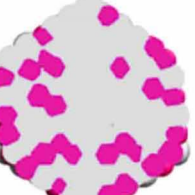
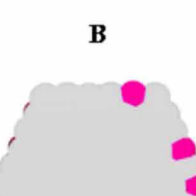

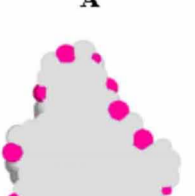
	Ico-type		Dec-type		TOh-type	
$\Delta\mu(\text{eV})$	Composition	Snapshot	Composition	Snapshot	Composition	Snapshot
+0.2	Co <sub>48</sub> Pt <sub>513</sub>		Co <sub>21</sub> Pt <sub>540</sub>		Co <sub>4</sub> Pt <sub>707</sub>	
+0.3	Co <sub>90</sub> Pt <sub>471</sub>		Co <sub>107</sub> Pt <sub>454</sub>		Co <sub>57</sub> Pt <sub>654</sub>	
+0.4	Co <sub>137</sub> Pt <sub>424</sub>		Co <sub>146</sub> Pt <sub>415</sub>		Co <sub>201</sub> Pt <sub>510</sub>	
+0.5	Co <sub>243</sub> Pt <sub>318</sub>		Co <sub>248</sub> Pt <sub>313</sub>		Co <sub>337</sub> Pt <sub>374</sub>	
+0.6	Co <sub>344</sub> Pt <sub>217</sub>		Co <sub>338</sub> Pt <sub>223</sub>		Co <sub>473</sub> Pt <sub>238</sub>	
+0.8	Co <sub>490</sub> Pt <sub>71</sub>		Co <sub>485</sub> Pt <sub>76</sub>		Co <sub>622</sub> Pt <sub>89</sub>	
		<b>B</b>				<b>A</b>

TABLE III. Average binding energy  $E_b$  for CoPt<sub>3</sub> NPs with Ico-type, Dec-type, and TOh-type morphologies at 100 K. Experimental value (Ref. 71) is also introduced for a comparison with our results.

	Ico-type Co <sub>0.25</sub> Pt <sub>0.75</sub>	Dec-type Co <sub>0.26</sub> Pt <sub>0.74</sub>	TOh-type Co <sub>0.28</sub> Pt <sub>0.72</sub>	Experimental value (Ref. 71)
$E_b$ /eV	5.37	5.34	5.33	5.33

$$\Delta E_{b(\text{Dec-Ico})} = E_{b(\text{Dec})} - E_{b(\text{Ico})}, \quad (10)$$

where  $E_{b(\text{Ico})}$  and  $E_{b(\text{Dec})}$  represent the average binding energy of Co-Pt bimetallic NPs with initial Ico-type and Dec-type morphologies, respectively.

To compare the relative stability of bimetallic NPs with different compositions, the relationship between  $\Delta E_{b(\text{Dec-Ico})}$  and Co mole fraction at 100 K are shown in Fig. 2. It is found that  $\Delta E_{b(\text{Dec-Ico})}$  is approximately equal to  $E_{b(\text{Ico})}$  at 0.00 Co mole fraction, showing that icosahedron and decahedron are competing intensely for the most stable structure. It is noticed that  $\Delta E_{b(\text{Dec-Ico})}$  increases to positive value at low Co mole fraction, indicating an increase in the average binding energy when a few Pt atoms are replaced by Co atoms in Dec-type NPs. However, with the Co mole fraction increases continuously,  $\Delta E_{b(\text{Dec-Ico})}$  decreases rapidly, especially in the range of 0.04–0.19.  $\Delta E_{b(\text{Dec-Ico})}$  transforms into negative values up to 0.07 Co mole fraction. Therefore, Dec-type NPs are more stable from 0.07 to 0.58 Co mole fraction. When Co mole fraction is more than 0.77,  $\Delta E_{b(\text{Dec-Ico})}$  changes dramatically, first fall rapidly and then rise fast. It should be mentioned that Dec-type NPs cannot keep a regular morphology in this range. It is also found that the order of structural stability is Dec-type and Ico-type morphologies in the pure Co NPs. However, the morphology transition from Ico-type to Dec-type is not observed in the snapshots. During the MC simulations, we have to monitor some necessary physical quantities to obtain the Co-Pt bimetallic NPs with different compositions, such as potential energy and the number of Co atoms in Co<sub>x</sub>Pt<sub>561-x</sub> or Co<sub>x</sub>Pt<sub>711-x</sub>. There are

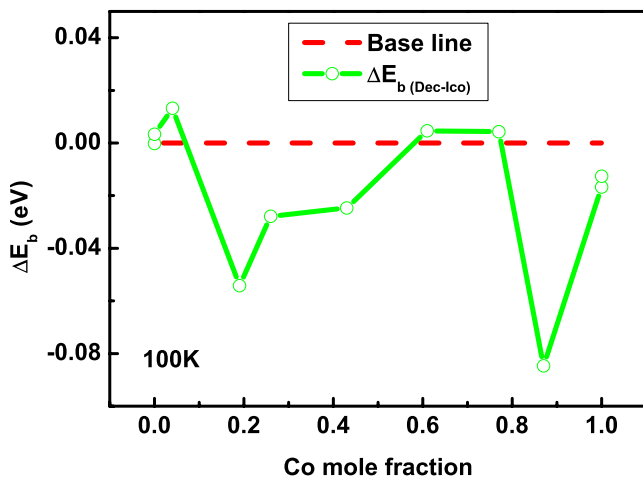


FIG. 2. (Color online)  $\Delta E_{b(\text{Dec-Ico})}$  versus Co mole fraction at 100 K.  $E_{b(\text{Ico})}$  is in red dashed line and set to 0 as a base line.  $\Delta E_{b(\text{Dec-Ico})}$  is in green circles line.

two other important parameters we have to pay attention to, that is, the overall acceptance rate for particles' displacements and changes of type. The two quantities are close to 50% and in the range of 0.5–20 %, respectively.<sup>72</sup>

### B. Analysis of PDFs with different morphologies

In order to study the structure of Co-Pt bimetallic NPs at atomic level, structure functions  $S(Q)$  are also calculated. Aiming at comparing with experimental result, the 1:1 atomic ratio Co-Pt bimetallic NPs are mainly discussed below. Structure functions  $S(Q)$  for total atom pairs with Ico-type, Dec-type, and TOh-type morphologies and about 0.50 Co mole fraction at 100 K are displayed in Fig. 3. It is found that there are only a few well-defined peaks due to the finite nanoscale size effect in NPs system. These peaks in the scattering patterns are very sensitive to the fivefold symmetrical structure in the Ico-type and Dec-type NPs. In the case of Ico-type NP in Fig. 3(b), one broad peak locating at  $3.05 \text{ \AA}^{-1}$  can be identified. When  $Q$  value is up to  $3.33 \text{ \AA}^{-1}$ , what is observed is only oscillating component.  $S(Q)$  of Dec-type NP shows less peaks while TOh-type  $S(Q)$  have four noticeable peaks positioned at  $2.97 \text{ \AA}^{-1}$ ,  $3.40 \text{ \AA}^{-1}$ ,  $4.84 \text{ \AA}^{-1}$ , and  $5.66 \text{ \AA}^{-1}$ , respectively. These peaks in  $S(Q)$  with TOh-type structure indicate a better local atom arrangement than other type NPs. It is also found that the first peaks

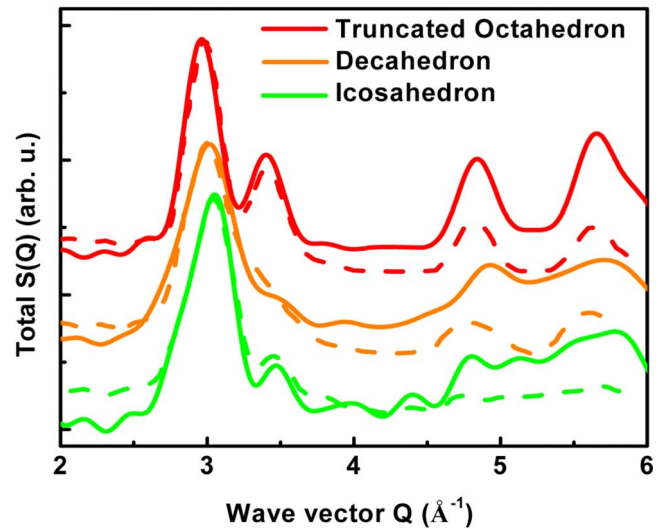


FIG. 3. (Color online) Calculated structure functions  $S(Q)$  for total atom pairs with Ico-type, Dec-type, and TOh-type morphologies and about 0.50 Co mole fraction at 100 K.  $S(Q)$  for total atom pairs is also compared with experimental result taken from Penuelas *et al.* (Ref. 13). Our calculated  $S(Q)$  is in solid lines and experimental result is in dashed lines.

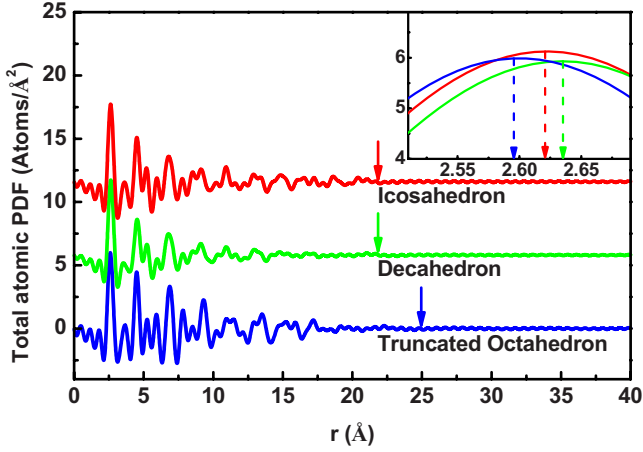


FIG. 4. (Color online) Calculated atomic PDFs for total atom pairs with three different morphologies and about 0.50 Co mole fraction at 100 K. First peaks of these curves are given as an inset on enlarged scale. The solid arrows represent the average size of Co-Pt bimetallic NPs (assuming spherical shape) while the dashed arrows correspond to the first-neighbor atom distances.

positions are different, that is,  $3.05 \text{ \AA}^{-1}$ ,  $3.02 \text{ \AA}^{-1}$ , and  $2.96 \text{ \AA}^{-1}$  for Ico-type, Dec-type, and TOh-type NPs, respectively. As expected, this is mainly due to the different atom arrangements in these NPs. Our computational  $S(Q)$  has a comparison with experimental scattering patterns,<sup>13</sup> which are also listed in Fig. 3. It is indicated that the structure functions  $S(Q)$  of simulation are in well agreement with the experimental data.<sup>13</sup> However, computational  $S(Q)$  values are slightly different from experimental values at low  $Q$  ( $\leq 2.65 \text{ \AA}^{-1}$ ) or high  $Q$  ( $\geq 3.65 \text{ \AA}^{-1}$ ), mainly caused by different NPs size. Furthermore, the structure functions  $S(Q)$  for Co-Co, Pt-Pt, and Co-Pt atom pairs can also be obtained by Eq. (8) and show similar characters to that for total atom pairs (see Fig. 12, Ref. 72). In general, such patterns are very difficult to be analyzed for obtaining atomic-level structural properties. Hence, a new technique called atomic PDF is adopted in this work to investigate the atomic arrangement of Co-Pt bimetallic NPs.

Atomic PDFs with three different morphologies are performed and shown in Fig. 4, which show several well-defined peaks below  $10.00 \text{ \AA}$ . Whereas, peaks of atomic PDFs reduce as the increase in interatomic distance  $r$  and even decay to zero up  $\sim 20.00 \text{ \AA}$  below the average particle size. The decays of the intensity in PDFs are mainly assigned to the finite nanoscale size effect (assuming spherical shape),

giving an idea of the so-called ‘‘coherent domain size’’ of the NPs. It should be mentioned that the first peak position corresponds to the first-neighbor atom distance. From the enlarged first peaks in Fig. 4, we can find that the first-neighbor atom distances are slightly different with Ico-type, Dec-type, and TOh-type morphologies. The shift of the first peak positions is also observed in the first-neighbor Co-Co, Pt-Pt, and Co-Pt distances (see Fig. 13, Ref. 72). To compare with experimental values of around 2 nm NPs and bulk, the first-neighbor Co-Co, Pt-Pt, and Co-Pt distances are summarized and listed in Table IV.

It is seen in Table IV that the first-neighbor Co-Co, Pt-Pt, and Co-Pt distances obtained through PDFs analysis are well consistent with experimental around 2 nm NPs, which has the similar size with our Co-Pt bimetallic NPs obtained through MC simulations.<sup>73</sup> In details, the first-neighbor Co-Co distances with Ico-type, Dec-type, and TOh-type morphologies are  $2.53 \pm 0.01 \text{ \AA}$ ,  $2.51 \pm 0.01 \text{ \AA}$ , and  $2.54 \pm 0.01 \text{ \AA}$ , respectively, which are very close to  $2.508(\pm 0.005) \text{ \AA}$  in experimental measurement.<sup>73</sup> The first-neighbor Co-Pt and Pt-Pt distances are in the range of  $2.57\text{--}2.58(\pm 0.01) \text{ \AA}$  and  $2.64\text{--}2.68(\pm 0.01) \text{ \AA}$ , respectively, which are both in agreement with 2 nm NPs of  $2.564(\pm 0.006) \text{ \AA}$  and  $2.670(\pm 0.005) \text{ \AA}$  in experimental study.<sup>73</sup> The well match of the first-neighbor atom distances between the model and experiment for the around 2 nm NPs validates the excellent employ of MC simulation and PDF methods to investigate the atomic-scale structural properties of bimetallic NPs in this study.

### C. Analysis of PDFs with different Co mole fractions

Aiming at understanding the composition effect on the atomic-scale structural properties, total atomic PDFs for different Co mole fractions are shown in Fig. 5. It is found that the PDFs for  $\text{Co}_{0.87}\text{Pt}_{0.13}$  (symbol ‘‘A’’) and  $\text{Co}_{0.77}\text{Pt}_{0.23}$  NPs show less features than others, that is, their peaks vanish at very short interatomic distance. This is mainly caused by the irregular structure of Co-Pt bimetallic NPs with  $\Delta\mu=0.7$  and  $0.8 \text{ eV}$ . On the other hand, it is found that the first peak positions shift from  $2.68$  to  $2.41 \text{ \AA}$  as the increase in Co mole fraction resulting from the substitution Pt atoms for smaller Co atoms. From the shift of the first peak positions, it can be validated that composition plays an important role in the first-neighbor Co-Co, Co-Pt, and Pt-Pt distances, which are summarized and plotted in Fig. 6 as following discussion.

TABLE IV. The first-neighbor Co-Co, Pt-Pt, and Co-Pt distances with three morphologies and about 0.50 Co mole fraction at 100 K. The first-neighbor atom distances for around 2 nm NPs (Ref. 73) and bulk in experiment are also presented.

	Ico-type $\text{Co}_{0.51}\text{Pt}_{0.49}$ ( $\text{\AA}$ )	Dec-type $\text{Co}_{0.50}\text{Pt}_{0.50}$ ( $\text{\AA}$ )	TOh-type $\text{Co}_{0.51}\text{Pt}_{0.49}$ ( $\text{\AA}$ )	Around 2 nm NPs $\text{Co}_{0.50}\text{Pt}_{0.50}$ (Ref. 73) ( $\text{\AA}$ )	Bulk
Co-Co	$2.53(\pm 0.01)$	$2.51(\pm 0.01)$	$2.54(\pm 0.01)$	$2.508(\pm 0.005)$	$2.507$ (pure Co) <sup>a</sup>
Co-Pt	$2.58(\pm 0.01)$	$2.57(\pm 0.01)$	$2.57(\pm 0.01)$	$2.564(\pm 0.006)$	
Pt-Pt	$2.66(\pm 0.01)$	$2.68(\pm 0.01)$	$2.64(\pm 0.01)$	$2.670(\pm 0.005)$	$2.775$ (pure Pt) <sup>a</sup>

<sup>a</sup>Reference 47.

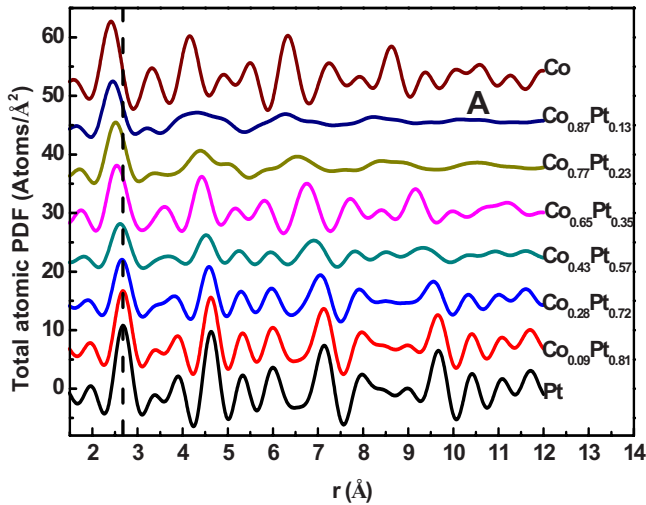


FIG. 5. (Color online) Calculated total atomic PDFs for different Co mole fractions with TOH-type morphology at 100 K. Symbol A represents  $\text{Co}_{622}\text{Pt}_{89}$  with an irregular structure in Table II.

To discuss the relationship between composition and first-neighbor atom distance, we present the first-neighbor Co-Co, Co-Pt, and Pt-Pt distances for different Co mole fraction at 100 K in Fig. 6. It is found in Fig. 6(a) that the first-neighbor Co-Co distance is  $2.51 \pm 0.01$  and  $2.50 \pm 0.01$  Å at 0.09 and 0.16 Co mole fractions and has a maximal value  $2.56 \pm 0.01$  Å at 0.25 Co mole fraction. The first-neighbor Co-Co distance begins to decrease as the Co mole fraction increases continuously. At last, the first-neighbor Co-Co distance for pure Co NP is  $2.42 \pm 0.01$  Å, which is smaller than that for bulk (2.507 Å). A similar change has been found in the first-neighbor Co-Pt distances, which are in the range of 2.52–2.62 ( $\pm 0.01$ ) Å. In the case of Pt-Pt, the first-neighbor distances are from 2.44 to 2.68 ( $\pm 0.01$ ) Å. It is also found that the first-neighbor Pt-Pt distance drops rapidly to  $2.44 \pm 0.01$  Å at point “B” in Fig. 6(a). As can be seen in Fig. 6(b), the first-neighbor Co-Co, Co-Pt, and Pt-Pt distances are 2.41–2.61 ( $\pm 0.01$ ) Å, 2.54–2.63 ( $\pm 0.01$ ) Å, and 2.66–2.68 ( $\pm 0.01$ ) Å, respectively. The first-neighbor atom distances with TOH-type morphology in Fig. 6(c) are 2.41–2.69 ( $\pm 0.01$ ) Å, 2.54–2.65 ( $\pm 0.01$ ) Å, and 2.62–2.68 ( $\pm 0.01$ ) Å, respectively. The first-neighbor Co-Co and Pt-Pt distances in pure Co and Pt NP are smaller than that in bulk (2.507 and 2.775 Å) due to the finite nanoscale size effect and crystal lattice contraction or distortion effect.<sup>5,24,73</sup> It should be noticed that there are nonsmooth transitions for the first-neighbor Co-Pt and Pt-Pt distances in the range of 0.51–0.77 Co mole fraction, because bimetallic NPs cannot keep regular morphologies.

In order to understand the quick drop at point B in Fig. 6(a), the snapshots of  $\text{Co}_{490}\text{Pt}_{71}$  and calculated atomic PDF for Pt-Pt atom pairs are shown in Fig. 7. It can be seen that the first peak splits and almost disappears while the second peak is much more visible. By analysis of the snapshots, we can find that Pt atoms are all separated on the surface and there are much more Pt atoms next to Co atoms rather than themselves. The very few Pt-Pt atom pairs in  $\text{Co}_{490}\text{Pt}_{71}$  result

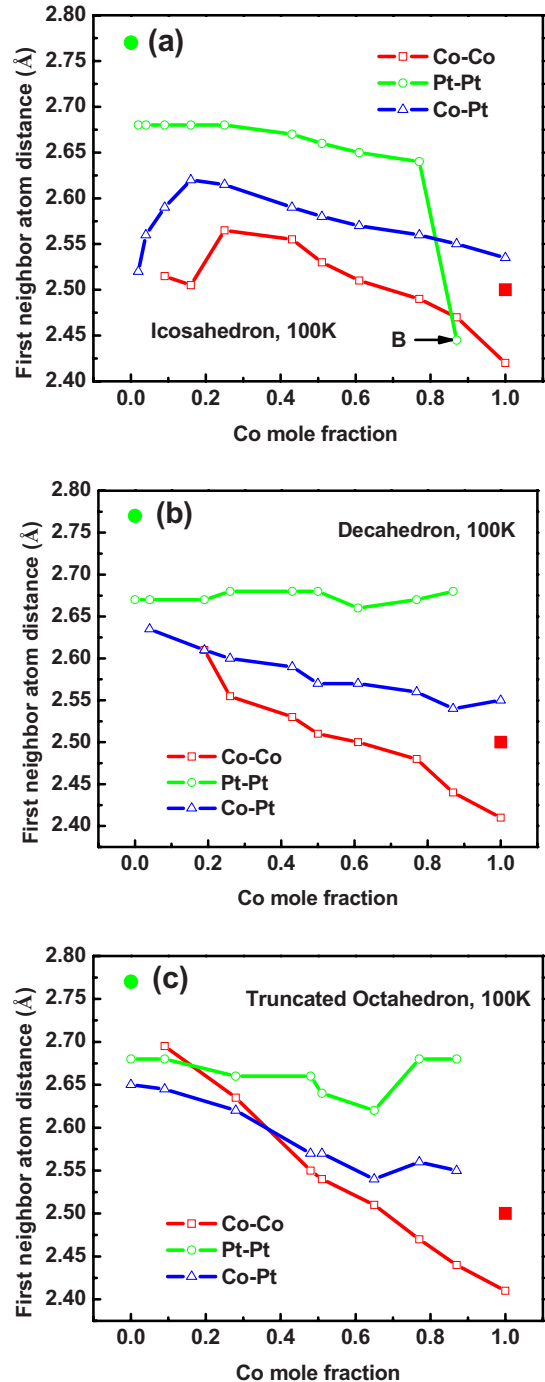


FIG. 6. (Color online) The first-neighbor Co-Co, Co-Pt, and Pt-Pt distances for different Co mole fractions with (a) Ico-type, (b) Dec-type, and (c) TOH-type morphologies at 100 K. Symbol B in (a) represents  $\text{Co}_{490}\text{Pt}_{71}$  in Table II. The first-neighbor atom distances for pure bulk Co and pure bulk Pt are 2.507 and 2.775 Å, which are presented in solid red square and green sphere, respectively.

in the vanishing of the first peak in Fig. 7, and the inaccuracy of the first-neighbor Pt-Pt distance at point B in Fig. 6(a).

#### D. Analysis of PDFs with different temperatures

It is well known that temperature plays an important role in the physicochemical properties of bimetallic materials.

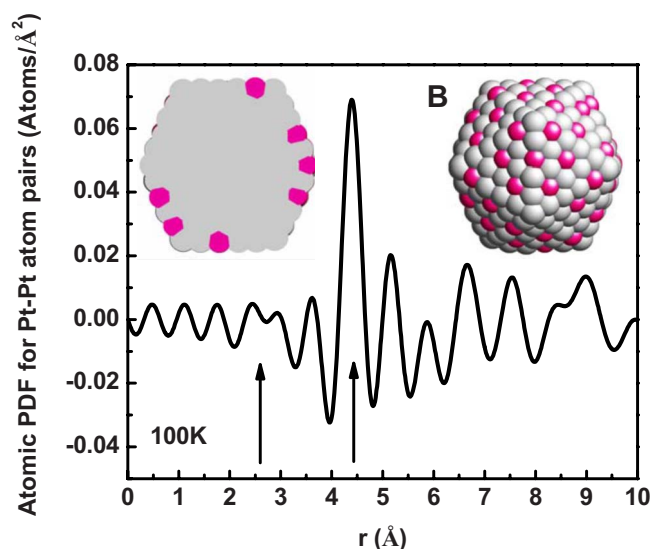


FIG. 7. (Color online) Snapshots of  $\text{Co}_{490}\text{Pt}_{71}$  and calculated atomic PDF for Pt-Pt atom pairs at 100 K. Symbol B represents  $\text{Co}_{490}\text{Pt}_{71}$  with Ico-type morphology in Table II. The left arrow should correspond to the first-neighbor Pt-Pt distance which seems disappeared while the right arrow corresponds to the second-neighbor Pt-Pt distance.

Therefore, atomic PDFs for total atom pairs with TOh-type morphology and about 0.50 Co mole fraction at 100, 300, and 500 K are also performed and shown in Fig. 8. By contrast, the first PDF peak at 100 K is sharper than that at 500 K, which is mainly caused by the weaker thermal vibration at lower temperature. Therefore, it is illustrated that temperature can exert an influence on the atomic-scale structural properties of bimetallic NPs. It is also found that the first-neighbor Co-Co, Co-Pt, and Pt-Pt distances are almost the same under the temperatures of 100, 300, and 500 K. In details, the first-neighbor Co-Co distances are  $2.55 \pm 0.01$  Å,  $2.55 \pm 0.01$  Å, and  $2.54 \pm 0.01$  Å at 100 K, 300 K, and 500 K, respectively. The first-neighbor Co-Pt distances are  $2.57 \pm 0.01$  Å,  $2.58 \pm 0.01$  Å, and  $2.59 \pm 0.01$  Å while the first-neighbor Pt-Pt distances are  $2.66 \pm 0.01$  Å,  $2.66 \pm 0.01$  Å, and  $2.67 \pm 0.01$  Å, respectively. The shift of the first-neighbor Co-Co, Co-Pt, and Pt-Pt distances is within error. The enlargement of the first-neighbor atom distances as the increase in temperature is not observed in this study, because the phenomenon of thermal expansion is always observed in experimental and theoretical studies at higher temperatures, which are generally around the melting point. What we adopt in our MC simulations is only lower temperatures, such as 100, 300, and 500 K.

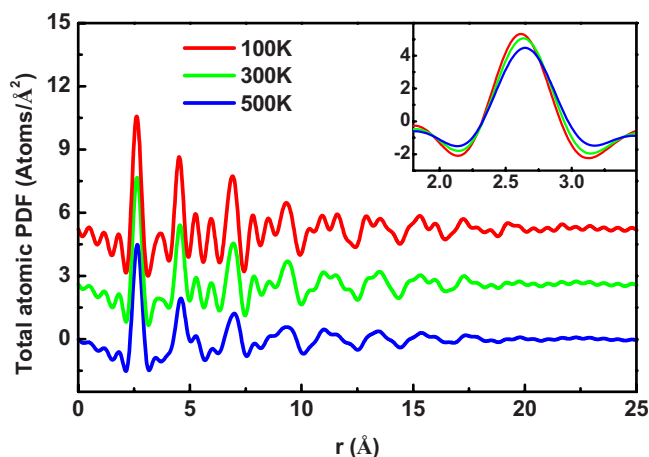


FIG. 8. (Color online) Calculated atomic PDFs for total atom pairs with TOh-type morphology and about 0.50 Co mole fraction at 100, 300, and 500 K. First peaks of these curves are given as an inset on enlarged scale.

## V. CONCLUSIONS

In summary, Co-Pt bimetallic nanoparticles with different morphologies, compositions and temperatures are obtained by using Monte Carlo simulation, which is based on the TB-SMA potential for the atom-atom interactions. The simulation results show that Co atoms prefer to occupy the inside and Pt atoms are generally lying on the surface of bimetallic NPs. As the increase in Co mole fraction, Co atoms occupy first the central site, then diagonal lines or adjacent vertices positions, finally the vertices and edges. Binding-energy difference is also performed to investigate the relative stability of Co-Pt bimetallic nanoparticles with different morphologies. All coordinates of simulation results are collected and transformed by the PDF technique into the atomic-scale structural properties. It is found that the first-neighbor Co-Co, Co-Pt, and Pt-Pt distances in the NPs with about 0.50 Co mole fraction at 100 K are  $2.51$ – $2.54$  ( $\pm 0.01$ ) Å,  $2.57$ – $2.58$  ( $\pm 0.01$ ) Å, and  $2.64$ – $2.68$  ( $\pm 0.01$ ) Å, respectively, which are all in agreement with experimental values of around 2 nm NPs. To sum up, morphology, composition, and temperature all play an important role in the atomic-level structural properties of Co-Pt bimetallic NPs.

## ACKNOWLEDGMENTS

This work is supported by the National Natural Science Foundation of China (Grant No. 20876005) and the National Basic Research Program of China (Grant No. 2010CB732301). Computational resources were supported by “Chemical Grid Project” of Beijing University of Chemical Technology.

\*Author to whom correspondence should be address. FAX: +86-10-64427616; huangsp@mail.buct.edu.cn

<sup>1</sup>J. Park, M. G. Kim, Y. Jun, J. S. Lee, W. Lee, and J. Cheon, *J. Am. Chem. Soc.* **126**, 9072 (2004).

<sup>2</sup>P. Snytnikov, K. Yusenkov, S. Korenev, Y. Shubin, and V. Soby-

nin, *React. Kinet. Catal. Lett.* **48**, 276 (2007).

<sup>3</sup>C. Kwak, T. J. Park, and D. J. Suh, *Appl. Catal., A* **278**, 181 (2005).

<sup>4</sup>U. A. Paulus, A. Wokaun, G. G. Scherer, T. J. Schmidt, V. Stamenkovic, V. Radmilovic, N. M. Markovic, and P. N. Ross, *J.*



- Phys. Chem. B* **106**, 4181 (2002).
- <sup>5</sup>U. A. Paulus, A. Wokaun, G. G. Scherer, T. J. Schmidt, V. Stamenkovic, N. M. Markovic, and P. N. Ross, *Electrochim. Acta* **47**, 3787 (2002).
- <sup>6</sup>S. K. Pradhan, Y. Mao, S. S. Wong, P. Chupas, and V. Petkov, *Chem. Mater.* **19**, 6180 (2007).
- <sup>7</sup>C. J. Lin and G. L. Gorman, *Appl. Phys. Lett.* **61**, 1600 (1992).
- <sup>8</sup>Y. Shibuta and T. Suzuki, *J. Chem. Phys.* **129**, 144102 (2008).
- <sup>9</sup>N. Toshima and T. Yonezawa, *New J. Chem.* **22**, 1179 (1998).
- <sup>10</sup>D. Cheng, W. Wang, and S. Huang, *J. Phys.: Condens. Matter* **19**, 356217 (2007).
- <sup>11</sup>J. L. Rodríguez-López, F. Aguilera-Granja, K. Michaelian, and A. Vega, *Phys. Rev. B* **67**, 174413 (2003).
- <sup>12</sup>P. Młynarski, M. Iglesias, M. Pereiro, D. Baldomir, and L. Wojtczak, *Vacuum* **54**, 143 (1999).
- <sup>13</sup>J. Penuelas, P. Andreazza, C. Andreazza-Vignolle, C. Mottet, M. De Santis, and H. C. N. Tolentino, *Eur. Phys. J. Spec. Top.* **167**, 19 (2009).
- <sup>14</sup>J. L. Rodríguez-López, J. M. Montejano-Carrizales, and M. José-Yacamán, *Mod. Phys. Lett. B* **20**, 725 (2006).
- <sup>15</sup>J. L. Rodríguez-López, J. M. Montejano-Carrizales, U. Pal, J. F. Sánchez-Ramírez, H. E. Troiani, D. García, M. Miki-Yoshida, and M. José-Yacamán, *Phys. Rev. Lett.* **92**, 196102 (2004).
- <sup>16</sup>J. M. Montejano-Carrizales, J. L. Rodríguez-López, U. Pal, M. Miki-Yoshida, and M. José-Yacamán, *Small* **2**, 351 (2006).
- <sup>17</sup>M. Zhang and R. Fournier, *Phys. Rev. A* **79**, 043203 (2009).
- <sup>18</sup>V. Kumar and Y. Kawazoe, *Phys. Rev. B* **77**, 205418 (2008).
- <sup>19</sup>F. Aguilera-Granja and A. Vega, *Phys. Rev. B* **79**, 144423 (2009).
- <sup>20</sup>F. Lai, L. S. Sarma, H. Chou, D. Liu, C. Hsieh, J. Lee, and B. Hwang, *J. Phys. Chem. C* **113**, 12674 (2009).
- <sup>21</sup>J. Thiele, N. T. Barrett, R. Belkhou, C. Guillot, and H. Koundi, *J. Phys.: Condens. Matter* **6**, 5025 (1994).
- <sup>22</sup>M. R. Visokay and R. Sinclair, *Appl. Phys. Lett.* **66**, 1692 (1995).
- <sup>23</sup>L. Cagnon, Y. Dahmane, J. Voiron, S. Pairis, M. Bacia, L. Ortega, N. Benbrahim, and A. Kadri, *J. Magn. Magn. Mater.* **310**, 2428 (2007).
- <sup>24</sup>L. Xiong and A. Manthiram, *J. Mater. Chem.* **14**, 1454 (2004).
- <sup>25</sup>A. C. C. Yu, M. Mizuno, Y. Sasaki, H. Kondo, and K. Hiraga, *Appl. Phys. Lett.* **81**, 3768 (2002).
- <sup>26</sup>D. Alloyeau, C. Ricolleau, C. Mottet, T. Oikawa, C. Langlois, Y. Le Bouar, N. Braidy, and A. Loiseau, *Nature Mater.* **8**, 940 (2009).
- <sup>27</sup>X. Du, M. Inokuchi, and N. Toshima, *J. Magn. Magn. Mater.* **299**, 21 (2006).
- <sup>28</sup>V. Petkov, *Synchrotron Radiat. News* **22**, 29 (2009).
- <sup>29</sup>N. Bedford, C. Dablemont, G. Viau, P. Chupas, and V. Petkov, *J. Phys. Chem. C* **111**, 18214 (2007).
- <sup>30</sup>V. Petkov, Y. Ren, I. Saratovsky, P. Pasten, S. J. Gurr, M. A. Hayward, K. R. Poepfelmeier, and J. F. Gaillard, *ACS Nano* **3**, 441 (2009).
- <sup>31</sup>M. Gateshki, V. Petkov, G. Williams, S. K. Pradhan, and Y. Ren, *Phys. Rev. B* **71**, 224107 (2005).
- <sup>32</sup>T. Proffen, K. L. Page, R. Seshadri, and A. Cheetham, *Los Alamos Sci.* **30**, 161 (2006).
- <sup>33</sup>V. Petkov, N. Bedford, M. R. Knecht, M. G. Weir, R. M. Crooks, W. Tang, G. Henkelman, and A. Frenkel, *J. Phys. Chem. C* **112**, 8907 (2008).
- <sup>34</sup>V. Petkov, P. Y. Zavalij, S. Lutta, M. S. Whittingham, V. Parvanov, and S. Shastri, *Phys. Rev. B* **69**, 085410 (2004).
- <sup>35</sup>W. Yao, S. W. Martin, and V. Petkov, *J. Non-Cryst. Solids* **351**, 1995 (2005).
- <sup>36</sup>V. Petkov, Y. Peng, G. Williams, B. Huang, D. Tomalia, and Y. Ren, *Phys. Rev. B* **72**, 195402 (2005).
- <sup>37</sup>S. K. Pradhan, Z. T. Deng, F. Tang, C. Wang, Y. Ren, P. Moeck, and V. Petkov, *J. Appl. Phys.* **102**, 044304 (2007).
- <sup>38</sup>D. L. Messurier, V. Petkov, S. W. Martin, Y. Kim, and Y. Ren, *J. Non-Cryst. Solids* **355**, 430 (2009).
- <sup>39</sup>Z. Lin and L. V. Zhigilei, *Phys. Rev. B* **73**, 184113 (2006).
- <sup>40</sup>M. Gateshki, S. Yin, Y. Ren, and V. Petkov, *Chem. Mater.* **19**, 2512 (2007).
- <sup>41</sup>V. Petkov, V. Parvanov, P. Trikalitis, C. Malliakas, T. Vogt, and M. G. Kanatzidis, *J. Am. Chem. Soc.* **127**, 8805 (2005).
- <sup>42</sup>B. B. Maranville, M. Schuerman, and F. Hellman, *Phys. Rev. B* **73**, 104435 (2006).
- <sup>43</sup>G. Rossi, R. Ferrando, and C. Mottet, *Faraday Discuss.* **138**, 193 (2008).
- <sup>44</sup>S. Rives, A. Catherinot, F. Dumas-Bouchiat, C. Champeaux, A. Videcoq, and R. Ferrando, *Phys. Rev. B* **77**, 085407 (2008).
- <sup>45</sup>R. J. Feng, X. H. Xu, and H. S. Wu, *J. Magn. Magn. Mater.* **308**, 131 (2007).
- <sup>46</sup>G. W. Turner, R. L. Johnston, and N. T. Wilson, *J. Chem. Phys.* **112**, 4773 (2000).
- <sup>47</sup>F. Cleri and V. Rosato, *Phys. Rev. B* **48**, 22 (1993).
- <sup>48</sup>J. Stanek, G. Marest, H. Jaffrezic, and H. Binczycka, *Phys. Rev. B* **52**, 8414 (1995).
- <sup>49</sup>A. Rapallo, G. Rossi, R. Ferrando, A. Fortunelli, B. C. Curley, L. D. Lloyd, G. M. Tarbuck, and R. L. Johnston, *J. Chem. Phys.* **122**, 194308 (2005).
- <sup>50</sup>F. Baletto, C. Mottet, A. Rapallo, G. Rossi, and R. Ferrando, *Surf. Sci.* **566-568**, 192 (2004).
- <sup>51</sup>M. Allalen, H. Bouzar, and T. Mehaddene, *Eur. Phys. J. B* **45**, 443 (2005).
- <sup>52</sup>J. Creuze, I. Braems, F. Berthier, C. Mottet, G. Tréglia, and B. Legrand, *Phys. Rev. B* **78**, 075413 (2008).
- <sup>53</sup>S. M. Foiles, *Phys. Rev. B* **32**, 7685 (1985).
- <sup>54</sup>S. M. Foiles, P. A. Dowben, and A. Miller, *Surface Segregation Phenomena* (CRC Press, Boca Raton, 1990).
- <sup>55</sup>P. Deurinck and C. Creemers, *Surf. Sci.* **419**, 62 (1998).
- <sup>56</sup>H. Q. Deng, W. Y. Hu, X. L. Shu, L. H. Zhao, and B. W. Zhang, *Surf. Sci.* **517**, 177 (2002).
- <sup>57</sup>H. Q. Deng, W. Y. Hu, X. L. Shu, and B. W. Zhang, *Surf. Sci.* **543**, 95 (2003).
- <sup>58</sup>J. A. Brown and Y. Mishin, *Phys. Rev. B* **67**, 195414 (2003).
- <sup>59</sup>M. Hou, V. S. Kharlamov, and E. E. Zhurkin, *Phys. Rev. B* **66**, 195408 (2002).
- <sup>60</sup>E. E. Zhurkin and M. Hou, *J. Phys.: Condens. Matter* **12**, 6735 (2000).
- <sup>61</sup>T. Van Hoof and M. Hou, *Appl. Surf. Sci.* **226**, 94 (2004).
- <sup>62</sup>A. V. Kazakov, E. S. Shpiro, and T. V. Voskoboinikov, *J. Phys. Chem.* **99**, 8323 (1995).
- <sup>63</sup>D. A. H. Cunningham, W. V. Sanchez, R. M. Torres, K. Tanaka, and M. Haruta, *J. Catal.* **183**, 24 (1999).
- <sup>64</sup>H. Zhang, B. Gilbert, F. Huang, and J. F. Banfield, *Nature (London)* **424**, 1025 (2003).
- <sup>65</sup>E. Prince, *International Tables for Crystallography* (P. J. Schmidt A/S, Denmark, 2004).
- <sup>66</sup>L. M. Peng, *Micron* **30**, 625 (1999).
- <sup>67</sup>W. Lee, M. G. Kim, J. Choi, J. Park, S. J. Ko, S. J. Oh, and J.

- Cheon, *J. Am. Chem. Soc.* **127**, 16090 (2005).
- <sup>68</sup>M. E. Gruner and P. Entel, *J. Phys.: Condens. Matter* **21**, 293201 (2009).
- <sup>69</sup>G. E. Ramírez-Caballero, Y. Ma, R. Callejas-Tovar, and P. B. Balbuena, *Phys. Chem. Chem. Phys.* **12**, 2209 (2010).
- <sup>70</sup>D. Cheng, S. Huang, and W. Wang, *Eur. Phys. J. D* **39**, 41 (2006).
- <sup>71</sup>R. Hultgren, P. D. Desai, D. T. Hawkins, M. Gleiser, and K. K. Kelley, *Selected Values of the Thermodynamic Properties of Binary Alloys* (Jossey-Bass, Berkeley, 1973).
- <sup>72</sup>See supplementary material at <http://link.aps.org/supplemental/10.1103/PhysRevB.82.075413> for the physical quantities monitored in the MC simulations.
- <sup>73</sup>B. J. Hwang, S. Kumar, C. H. Chen, M. Y. Cheng, Monalisa, D. G. Liu, and J. F. Leel, *J. Phys. Chem. C* **111**, 15267 (2007).